Radiative association of HeH_2^+

Felicja Mrugała[a)]
Institute of Physics, Nicolaus Copernicus University, Grudziadzka 5, PL 87-100 Torun, Poland

Vladimír Špirko
J. Heyrovský Institute of Physical Chemistry, Academy of Sciences of the Czech Republic and Center for Complex Molecular Systems and Biomolecules, Dolejškova 8, CZ 182 23 Prague, Czech Republic

Wolfgang P. Kraemer
Max-Planck-Institute of Astrophysics, Postfach 1317, D-85741 Garching, Germany

(Received 23 December 2002; accepted 18 March 2003)

Rigorous state-to-state quantum calculations of the dynamics of the radiative association reaction $He+H_2^+ \rightarrow HeH_2^+ + h\nu$ are performed. For this purpose the appropriate methodology is described in detail and computational aspects facilitating the actual calculations of the resonances and the free-bound phototransition amplitudes are discussed. Under the assumptions that the reaction is a single-state process proceeding entirely on the ground electronic state potential energy surface of HeH_2^+ and that higher dissociation channels of the ion complex can be neglected, all resonances contributing to the association are determined and the rate constant as a function of temperature is calculated for the low-temperature interval $2 \leqslant T \leqslant 100$ K. Its maximum value is predicted to be small, 2.1×10^{-20} cm^3s^{-1} at a temperature of about 20 K. © *2003 American Institute of Physics*. [DOI: 10.1063/1.1573184]

I. INTRODUCTION

The dynamical processes in low-energy ion–molecule collisions of various combinations of hydrogen atoms and molecules (both neutral and ionic) with helium ions or atoms have been studied intensively in the past because the $[HeH_2]^+$ ensemble is one of the most simple many-electron systems which allows for direct comparisons between experiments and high-level theoretical treatments.[1] It has also been argued that a comprehensive knowledge of these processes can provide theoretical rationales for various phenomena observed in astrophysical environments since hydrogen and helium are the most abundant interstellar elements.[2]

A number of experiments were performed to determine reaction rates for different exothermic inelastic processes occurring in $He^+ + H_2$ collisions under conditions simulating astrophysical environments,[3–5] and absolute rate constants at ultralow energies for some of these processes were measured by Schauer *et al.*[6] In $He+H_2^+$ collisions the endothermic proton abstraction process leading to the formation of HeH^+ is of some interest in primordial gas models because the reverse exothermic process could be an efficient depletion reaction for HeH^+. It has been studied experimentally (see, e.g., Ref. 7) and has received intensive theoretical attention over the past few years (see Refs. 8, 9, and references therein).

Due to the experimental difficulties to produce stable HeH_2^+ ions in their ground electronic state, reliable high-resolution spectroscopic information for the bound rovibrational energy levels is still missing. Only for some transitions between highly excited rovibrational levels close to the dissociation limit microwave spectral observations were reported by Carrington and co-workers.[10–12] Attempts to assign these transitions with the help of some of the best at that time existing *ab initio* potential energy surfaces for the ground electronic state were essentially unsuccessful due to deficiencies in the theoretical description, especially of the long- and the anisotropic short-distance interactions between He and H_2^+. These failures have triggered a number of recent theoretical attempts to evaluate more reliable interaction potentials for the HeH_2^+ system[13,14] and to improve that part of the ground-state potential which represents the HeH^+ formation-destruction reaction $He+H_2^+ \rightleftharpoons HeH^+ + H$.[9] Most recently, calculations on an accuracy level similar to that in Refs. 13 and 14 were completed in which the potential energy surfaces of the ground- and first excited states of HeH_2^+ were determined simultaneously.[15] Accurate potentials for both electronic states are needed to investigate the radiative charge transfer reaction

$$He^+ + H_2 \rightarrow He + H_2^+ + h\nu, \tag{1}$$

which could be of considerable interest in primordial gas models because it has a rather large cooling effect.

Making use of the ground electronic state results of these recent *ab initio* calculations,[15] the present study gives a detailed state-to-state description of the dynamics of the low-temperature radiative association reaction

$$He + H_2^+ \rightarrow HeH_2^+ + h\nu. \tag{2}$$

Due to the low binding energy of the HeH_2^+ association complex, the rate constant of this reaction can be expected to be rather small. However, the reaction is used here as a conve-

a)Electronic mail: felicja@phys.uni.torun.pl

nient first test case on which the present theory for triatomic association processes can be applied. For this purpose and as a reference for later studies of the more complicated radiative charge transfer reaction (1), a complete overview of the methodology is presented here and some computational aspects in the calculations of resonances (and their contributions to the rate constants) and in evaluating transition amplitudes are discussed.

In the present calculations it can be safely assumed that the association reaction (2) is completely determined by the ground-state potential of the HeH_2^+ complex. The ground state is well separated from the first excited state having the same symmetry, and there are no nonadiabatic couplings between them[16] over the entire range of geometries relevant for the association reaction at low temperatures. Such a process is therefore called a single-state process. A further assumption made in this study is that the existence of the higher dissociation channel leading to $HeH^+ + H$ can be neglected because it opens at an energy exceeding by far the collision energies considered here. Finally, it is assumed that the coupling of the electronic and nuclear spin states with the angular momentum states can be ignored because the effects due to this coupling are too small to be relevant for the present purpose.[14]

Apart from a number of rigorous quantal studies of the dynamics and rate constants of atomic radiative association reactions,[17] theoretical treatments of these processes in polyatomic systems are so far essentially based on the phase space approach[18,19] or statistical rate theory.[20] These theories are mostly not able to account in detail for quantum-phenomena and their contributions to the process. They should therefore be supported by truly quantum-mechanical calculations. The present paper presents the first rigorous detailed quantum state-to-state study of a triatomic atom–diatom radiative association reaction. It is the first one of a series of forthcoming studies of such processes in the weakly interacting $He+H_2^+$ and $He^+ + H_2$ systems and in other more strongly bound atom–diatom systems which are now in progress.

II. FORMULA FOR THE ASSOCIATION RATE CONSTANT

In order to derive the expression for the rate constant of the association reaction (2), we consider here a gas at thermal equilibrium with temperature T containing N_{He} He atoms and $N_{H_2^+}$ H_2^+ ions. The number of $He+H_2^+$ pairs in the gas that occupy a given state $|i\rangle$ of ro-vibro-translational motion in the center-of-mass reference frame is given by $N_i(T)=p_i(T)N_{He}N_{H_2^+}=VP_i(T)\,n_{He}n_{H_2^+}$, where $p_i(T)$ gives the occupation probability of the state $|i\rangle$, V is the volume of the gas sample, $n_{He}=N_{He}/V$ and $n_{H_2^+}=N_{H_2^+}/V$ are the respective number densities. The number density $n_{HeH_2^+}$ of HeH_2^+ ions in the gas which are formed in reaction (2) increases then as

$$\frac{d}{dt}n_{HeH_2^+}=k(T)\,n_{He}n_{H_2^+}, \tag{3}$$

where $k(T)$ is the *radiative association rate constant*. Assuming $R_{f\leftarrow i}$ to be the rate of transition of a $He+H_2^+$ pair from a continuum state $|i\rangle$ to a bound state $|f\rangle$ due to spontaneous emission in the atom–diatom association, this rate constant can be expressed as

$$k(T)=\sum_f \sum_i R_{f\leftarrow i}P_i(T). \tag{4}$$

The rate $R_{f\leftarrow i}$ is given by the following golden rule-like expression[21] (accounting for the matter–radiation interaction in first order of perturbation theory and assuming the electric dipole approximation for this interaction)

$$R_{f\leftarrow i}=\frac{2\pi}{\hbar}\sum_{q\nu}\frac{\hbar\omega_q}{2\varepsilon_0\mathcal{V}}|\langle f|\boldsymbol{\epsilon}_q^\nu\cdot\boldsymbol{d}|i\rangle|^2\delta(E_f-E_i-\hbar\omega_q), \tag{5}$$

where $\boldsymbol{d}$ is the electric dipole moment of the $He+H_2^+$ system, $\boldsymbol{q}$, $\boldsymbol{\epsilon}_q^\nu$ for $\nu=1,2$, and $\omega_q=cq$ denote, respectively, the wave vector, the polarization vectors, and the frequency in one mode of the emitted radiation, c is the speed of light, $\mathcal{V}$ is the cavity volume, and ε_0 is the electric permittivity in free space ($1/4\pi$ in electrostatic units). E_i and E_f are the energies of the initial and final molecular states, $|i\rangle$ and $|f\rangle$, respectively.

The Hamiltonian of nuclear motion of the $He+H_2^+$ system in the center-of-mass reference frame can be expressed as $H=H_0+\overline{V}$, where H_0 describes the motion of noninteracting He and H_2^+ subunits and $\overline{V}$ is the interaction potential. The Hamiltonian is most conveniently represented in the space-fixed (SF) reference frame using Jacobi coordinates, r, $(\theta_r,\phi_r):=\hat{\boldsymbol{r}}$, R, $(\theta_R,\phi_R):=\hat{\boldsymbol{R}}$, which denote the lengths, the spherical, and azimuthal angles between the vectors $\boldsymbol{r}$ and $\boldsymbol{R}$ joining, respectively, the nuclei in H_2^+ and the nuclear center of mass of this ion with the He nucleus. In these coordinates H_0 consists of two commuting operators, $H_0(\boldsymbol{r},\boldsymbol{R})=K_{He-HH}(\boldsymbol{R})+H_{HH^+}(\boldsymbol{r})$, where $K_{He-HH}(\boldsymbol{R})$ is the kinetic energy operator of the relative $He-H_2^+$ motion

$$K_{He-HH}(\boldsymbol{R})=\frac{-\hbar^2}{2\mu}\boldsymbol{\Delta}_{\boldsymbol{R}}=\frac{1}{2\mu}p^2(R)+\frac{1}{2\mu R^2}\boldsymbol{l}^2(\hat{\boldsymbol{R}}),$$

with $p(R)$ and $\boldsymbol{l}$ denoting the radial and angular momenta operators, and μ being the reduced mass of $He+H_2^+$, and $H_{HH^+}(\boldsymbol{r})$ is the Hamiltonian of the rovibrational motion of H_2^+. This Hamiltonian can be expressed again as $H_{HH^+}(\boldsymbol{r})=K_{H-H}(\boldsymbol{r})+V_{HH^+}(r)$, where $K_{H-H}(\boldsymbol{r})$ involves now the operators $p(r)$, and $\boldsymbol{J}(\hat{\mathbf{r}})$, and the reduced mass of H_2^+.

Continuum states of H, or strictly speaking, the stationary scattering states of outgoing wave type being of interest here, are defined by referring to states of H_0 with a definite momentum of the $\boldsymbol{R}$ motion, $\langle\boldsymbol{R}r\hat{\mathbf{r}}|E\hat{\mathbf{k}}vjm_j\rangle=\sqrt{\rho}\exp\boldsymbol{k}\cdot\boldsymbol{R}\langle r\hat{\mathbf{r}}|vjm_j\rangle$, where $\hat{\boldsymbol{k}}$ denotes the direction of the wave vector $\boldsymbol{k}$ whose length is $k_{vj}(E)=\sqrt{(2\mu/\hbar^2)(E-\varepsilon_{vj})}$, ε_{vj} denotes the energy of the $|vjm_j\rangle$ state of H_{HH^+} with v and j being the vibrational and rotational quantum numbers, respectively, and m_j is the quantum number associated with the operator j_z (the projection of the

rotational angular momentum of H_2^+ on space-fixed z axis). The factor $\sqrt{\rho}=\sqrt{\mu\hbar k_{vj}/(2\pi\hbar)^3}$ assures energy normalization of the states

$$\int d\hat{\boldsymbol{k}}\langle v'j'm_j'|\langle E'\hat{\boldsymbol{k}}'|E\hat{\boldsymbol{k}}\rangle|vjm_j\rangle=\delta(E-E')\,\delta_{vjm_j;v'j'm_j'}. \tag{6}$$

The scattering state of H which evolves from the state $|E\hat{\boldsymbol{k}}vjm_j\rangle$ (under the action of the Moeller operator Ω^+, cf. Refs. 22, 23) is denoted by $|E^+,\hat{\boldsymbol{k}}vjm_j\rangle$ where the symbols behind the comma refer to quantum numbers which are not preserved by the interaction $\overline{V}$.

Thus, $|\mathrm{i}\rangle:=|E^+,\hat{\boldsymbol{k}}vjm_j\rangle$ and the sum over the initial state in Eq. (4) should be understood as $\Sigma_\mathrm{i}:=\int dE\int d\hat{\boldsymbol{k}}\Sigma_{vj}\Sigma_{m_j}$. The final state ket is specified as $|\mathrm{f}\rangle:=|E^BJ^BM^Bp^B\rangle$, accounting for the fact that bound states of H are simultaneous eigenstates of the operators $\boldsymbol{J}^2=(\boldsymbol{j}+\boldsymbol{l})^2$, J_z, and of the spatial inversion operator $\mathcal{I}$ with eigenvalues $\hbar^2J^B(J^B+1)$, $\hbar M^B$, and $(-1)^{J^B}p^B$, respectively. The sum over the final states therefore involves summation over different bound state energy levels and summation over magnetic substates $\Sigma_\mathrm{f}:=\Sigma_\mathcal{B}\Sigma_{M^B}$. Obviously, the index $\mathcal{B}$ is a composite one. Besides the good quantum numbers J^B and p^B, it includes four approximate quantum numbers which can possibly be utilized to identify energy levels of HeH_2^+.

Now, use can be made of the expansion of the scattering state $|E^+,\hat{\boldsymbol{k}}vjm_j\rangle$ into partial states[22,23] $|E^+JMp,vjl\rangle$ having well-defined quantum numbers J, M, and $p=(-1)^{j+l+J}$ related to the operators $\boldsymbol{J}^2$, J_z, and $\mathcal{I}$, respectively

$$|E^+,\hat{\boldsymbol{k}}vjm_j\rangle=\sum_{JM}\sum_{p=\pm1}\sum_{l(p)}|E^+JMp,vjl\rangle \times\sum_{m_l} i^lC(jlJ,m_jm_lM)Y^\star_{lm_l}(\hat{\boldsymbol{k}}). \tag{7}$$

Here, l is the angular momentum quantum number of the relative motion, the sum over $l(p)$ runs in steps of 2 from $|J-j|+(1-p)/2$ to $J+j$, the symbol $C(\ldots,\ldots)$ denotes the Clebsch–Gordan coefficient, and Y represents spherical harmonics. Applying the Wigner–Eckart theorem,[24] one can show that (see, e.g., Refs. 25, 26)

$$\sum_{m_j}\sum_{M^B}\int d\hat{\boldsymbol{k}}|\langle E^BJ^BM^Bp^B|\boldsymbol{\epsilon}^\nu_{\boldsymbol{q}}\cdot\boldsymbol{d}|E^+,\hat{\boldsymbol{k}}vjm_j\rangle|^2 =\frac{1}{3}\sum_{Jp}(2J+1)\sum_{l(p)}|T_{vjl}(E^BJ^Bp^B;EJp)|^2,$$

where $T_{vjl}(E^BJ^Bp^B;EJp)$ denotes the reduced free↔bound phototransition amplitude. When this quantity is nonzero, i.e., for $J=J^B$, $J^B\pm1$, and $p=p^B(-1)^{J+J^B+1}$, it is defined as

$$T_{vjl}(E^BJ^Bp^B;EJp):=\sqrt{\frac{2J^B+1}{2J+1}}\frac{\langle E^BJ^BM^Bp^B|d_\mu|E^+JMp,vjl\rangle}{C(J1J^B,M\mu M^B)}, \tag{8}$$

where d_μ for $\mu=0,\pm1$ denote spherical components of the vector $\boldsymbol{d}$, $d_0=d_z$, and $d_{\pm1}=\mp(1/\sqrt{2})(d_x\pm id_y)$.

After performing the operations $\Sigma_{m_j}\Sigma_{M^B}\int d\hat{\boldsymbol{k}}$ in the expressions for the rate constant Eqs. (4)–(5), the summation over the radiation modes is done in the usual manner,[21] i.e., by replacing: $\Sigma_{\boldsymbol{q}\nu}\to\mathcal{V}/(\pi^2c^3)\int\omega\boldsymbol{q}^2d\omega\boldsymbol{q}$. Finally, the appropriate population factor $P_\mathrm{i}(T)$ which has to be inserted into Eq. (4) is given by[27]

$$P^I(E,T)=\lambda^3(T)\frac{\exp\left(-\frac{E}{k_BT}\right)g^I}{Z_\mathrm{int}(T)},$$

with

$$Z_\mathrm{int}(T)=\sum_{vj}g_j(2j+1)\exp\left(-\frac{\varepsilon_{vj}}{k_BT}\right),$$

where $\lambda=\sqrt{2\pi\hbar^2/\mu k_BT}$ is the thermal de Broglie wavelength associated with the relative motion, k_B is the Boltzmann constant, g^I is the statistical weight of the nuclear spin states of H_2^+, $g^I=1/4,3/4$ for $I=0,1$, $g_j=g^0$ and $g_j=g^1$ for j even and j odd, respectively.

The resulting rate constant for the formation of the HeH_2^+ ion can then be written as the sum

$$k(T)=k^0(T)+k^1(T),$$

where the terms $k^I(T)$ $(I=0,1)$ describe formation of *para* and *ortho* HeH_2^+ ions, respectively, and the formula for them reads

$$k^I(T)=\sum_\mathcal{B}\sum_{Jp}(2J+1)\int dEP^I(E,T)\frac{\partial R^I(\mathcal{B};EJp)}{\partial E} \tag{9}$$

with

$$\frac{\partial R^I(\mathcal{B};EJp)}{\partial E}:=\frac{4}{3c^3\hbar^4}(E-E^B)^3\boldsymbol{T}^{I\dagger}_{\mathrm{B}\leftrightarrow\mathrm{F}}\boldsymbol{T}^I_{\mathrm{B}\leftrightarrow\mathrm{F}}(E^BJ^Bp^B;EJp).$$

$\boldsymbol{T}^I_{\mathrm{B}\leftrightarrow\mathrm{F}}$ denotes a column vector containing the reduced phototransition amplitudes T_{vjl} with j even (odd) for $I=0(1)$. Obviously, the rate constant $k^I(T)$ can be further resolved according to

$$k^I(T)=\sum_\mathcal{B}\sum_{vj}k^I_{\mathcal{B}\leftarrow vj}(T), \tag{10}$$

into the terms

$$k^I_{\mathcal{B}\leftarrow vj}(T)=\int dEP^I(E,T)\frac{\partial R^I(\mathcal{B};E,vj)}{\partial E},$$

where the quantity $[\partial R^I(\mathcal{B};E,vj)]/\partial E\,dE$ has the meaning of the rate of formation of the $HeH_2^+(I)$ ion in a defined state $\mathcal{B}$ when the total energy (in the center of mass) of the initially unbound and noninteracting $He+H_2^+$ system is between E and $E+dE$ and part of this energy, ε_{vj}, is the rovibrational energy of the diatomic subunit.

Equivalently, the $\mathcal{B}\leftarrow vj$ transitions can be described by the cross sections $\sigma^I_{\mathcal{B}\leftarrow vj}(E)$, defined through the relation[27]

$$\frac{\partial R^I(\mathcal{B};E,vj)}{\partial E}=4\pi v(E-\varepsilon_{vj})\rho(E-\varepsilon_{vj})\sigma^I_{\mathcal{B}\leftarrow vj}(E),$$

where $v(e)$ denotes velocity of the translational motion of energy $e=E-\varepsilon_{vj}$ and $\rho(e)$ is the energy density of translational states per unit volume; $4\pi v\rho=k_{vj}^2/(\pi h)$. In terms of the reduced phototransition amplitudes (8), the formula for $\sigma^I_{\mathcal{B}\leftarrow vj}(E):=\Sigma_{Jp}(2J+1)\sigma^I_{\mathcal{B}\leftarrow vj}(EJp)$ reads

$$\sigma^I_{\mathcal{B}\leftarrow vj}(EJp)=\frac{\pi}{k_{vj}^2}\frac{64\pi^4}{3h^3c^3}(E-E^B)^3\sum_{l(p)}|T^I_{vjl}(\mathcal{B};EJp)|^2. \tag{11}$$

Using this cross section, we can rewrite the expression for the rate constant $k_{\mathcal{B}\leftarrow vj}(T)$ as

$$k^I_{\mathcal{B}\leftarrow vj}(T)=p^I_{vj}(T)\int_0^\infty w(e,T)de\sqrt{\frac{2e}{\mu}}\sigma^I_{\mathcal{B}\leftarrow vj}(e+\varepsilon_{vj}), \tag{12}$$

where $p^I_{vj}(T)=Z_{\rm int}^{-1}g^I\exp(-\varepsilon_{vj}/k_BT)$ is the occupation probability of the internal vj state and $w(e,T)de=2\pi/(\pi k_BT)^{3/2}\sqrt{e}\exp(-e/k_BT)de$ is the probability distribution of the energy of the relative motion in the canonical ensemble at temperature T.

The expressions for the cross section $\sigma^I_{\mathcal{B}\leftarrow vj}(E)$ and the rate constant $k^I_{\mathcal{B}\leftarrow vj}(T)$ derived here for atom–diatom systems are the equivalents of the corresponding quantities used in the description of atom-atom radiative association (cf. Ref. 28).

III. RESONANCE CONTRIBUTION TO THE ASSOCIATION RATE CONSTANT

There are many long-living quasibound states (resonances) of the $He+H_2^+$ pairs in the low collision energy range, and is it known from theoretical considerations, cf. Refs. 29–31, and from a number of atomic association calculations[32–35] that these resonances can enhance the association rates significantly. Some care therefore has to be used to take their contributions to the association rate constant $k(T)$ properly into account.

Resonances manifest themselves in the rapidly changing energy dependence of the rates $[\partial R(\mathcal{B};EJp)]/\partial E$ [or the photoassociation cross sections $\sigma_{\mathcal{B}\leftarrow vj}(EJp)$]. Obviously, this complicates the evaluation of the integral in Eq. (9). Very long-living resonances (extremely sharp structures in the respective energy functions) require a special treatment, not only for technical reasons, cf. Refs. 30, 32. When the probabilities for the decay of such resonances due to molecular interactions become comparable to the probabilities of their decay due to interaction with a radiation field, these two decay pathways can no longer be treated completely independent from each other. This fact has been accounted for in the formula for the resonance contributions to the association rate constant published by Bain and Bardsley in their early 1972 paper,[31]

$$k^{\rm res}(T)=\frac{1}{\hbar}\sum_n P(E_n^{\rm res},T)(2J_n+1)\Gamma^n_{\rm rad}\frac{\Gamma_n}{\Gamma^n_{\rm rad}+\Gamma_n}, \tag{13}$$

where the index n counts the contributing resonances. This formula has been widely used since then in many calculations of atomic radiative association processes.

In order to apply the Bain–Bardsley formula to the present study, it is helpful to summarize the approximations on which it is based. The first approximation made is to neglect initially the radiation field and to apply the standard isolated resonance model,[36–38] i.e., it is assumed that all the sharp resonances are separated from each other and that they do not overlap. The partial scattering state $|E^+JMp,vjl\rangle$ which becomes dominant and rapidly varying with energy in the vicinity of a resonance can then be approximated as

$$|E^+JMp,vjl\rangle\approx|E^{B_Q}JMp\rangle_Q a^{Jp}_{vjl}(E)$$

with

$$a^{Jp}_{vjl}(E)=\frac{1}{\sqrt{2\pi}}\frac{\gamma^{Jp}_{vjl}}{E-E^{\rm res}+\frac{i}{2}\Gamma}, \tag{14}$$

where $|E^{B_Q}JMp\rangle_Q$ denotes a bound-type eigenstate of the Hamiltonian H projected onto an appropriate subspace Q.[38] The corresponding eigenenergy E^{B_Q} is assumed to be close to the energy of the resonance, $E^{\rm res}$. The associated resonance width is given by $\Gamma=\Sigma_{vjl}|\gamma^{Jp}_{vjl}|^2$. As a consequence of this approximation, a Lorentzian profile is obtained for the energy-differential association rate

$$\frac{\partial R(\mathcal{B};EJp)}{\partial E}\approx\frac{1}{\hbar}\Gamma^{Jp}_{{\rm rad},\mathcal{B}}\frac{\Gamma/2\pi}{(E-E^{\rm res})^2+\left(\frac{\Gamma}{2}\right)^2}, \tag{15}$$

where the parameter $\Gamma^{Jp}_{{\rm rad},\mathcal{B}}$ of the profile is defined as

$$\Gamma^{Jp}_{{\rm rad},\mathcal{B}}:=\frac{4}{3c^3\hbar^3}(E^{\rm res}-E^B)^3|T(\mathcal{B};E^{B_Q}Jp)|^2, \tag{16}$$

with $T(\mathcal{B};E^{B_Q}Jp)$ denoting the reduced phototransition amplitude which is obtained when the state $|E^{B_Q}JMp\rangle_Q$ is inserted into Eq. (8) in place of $|E^+JMp,vjl\rangle$. Obviously, $\Gamma^{Jp}_{{\rm rad},\mathcal{B}}/\hbar$ is a measure of the rate of radiative decay of the resonance into state $\mathcal{B}$. The quantity

$$\Gamma_{\rm rad}:=\sum_{\mathcal{B}}\Gamma^{Jp}_{{\rm rad},\mathcal{B}}, \tag{17}$$

is therefore called the radiative width of the resonance. Integration over the energy of the profile (15) with a very small width Γ would give according to Eq. (9) the following estimate of the contribution of the corresponding resonance to the rate constant $k(T)$: $k^{\rm res}(T)\approx P(E^{\rm res},T)(2J+1)\times(1/\hbar)\Gamma_{\rm rad}$. In this estimate every resonance can participate in the radiative association process, no matter how long is its lifetime for nonradiative decay, $\hbar/\Gamma$. But, this would not be consistent with the assumed kinetics of the process which is based on the requirement that the concentration of resonances in the gas has to be in thermal equilibrium with the concentration of the reactants. (cf. Ref. 30 for a discussion of this point). In order to correct this inconsistency, the interaction with the radiation field is now incorporated into the approximate resonance state description of Eq. (14) making use of the implicit optical potential approach of Ref. 29, i.e., the real energy $E^{\rm res}$ is replaced with the complex value $E^{\rm res}-(i/2)\Gamma_{\rm rad}$. This leads finally to the above Bain–Bardsley

formula of Eq. (13). The additional factor $\Gamma_n/(\Gamma_{\rm rad}^n+\Gamma_n)$ in this expression becomes effective if Γ_n is comparable to or much smaller than $\Gamma_{\rm rad}^n$.

IV. DETERMINATION OF FREE-BOUND PHOTOTRANSITION AMPLITUDES

For the discussions of this section, the expression of Eq. (8) defining the transition amplitudes is rewritten here in the more explicit form

$$\boldsymbol{T}_{\rm B\leftrightarrow F}(E^B J^B p^B;EJp) = \sqrt{\frac{2J^B+1}{2J+1}} \times \frac{\langle \Psi^{(B)}{}_{J^B M^B p^B}(E^B;\boldsymbol{r},\boldsymbol{R})|d_\mu(\boldsymbol{r},\boldsymbol{R})\Psi^{(+)}{}_{JMp}(E;\boldsymbol{r},\boldsymbol{R})\rangle}{C(J1J^B,M\mu M^B)}.$$

$\boldsymbol{\Psi}^{(+)}{}_{1\times N_{\rm o}}^{JMp}(E;\boldsymbol{r},\boldsymbol{R})$ denotes here the set of the partial scattering outgoing waves, $\langle \boldsymbol{r},\boldsymbol{R}|E^+JMp,\alpha_i\rangle$ for $i=1,\ldots,N_{\rm o}$, which correspond to all open scattering channels, i.e., $N_{\rm o}=N_{\rm o}(E,J,p)$ is the number of different α's, $\alpha:=(v,j,l)$, which for the given energy E, total angular momentum J, and parity p, are consistent with the angular momentum addition rules and with the requirement that $\epsilon_{vj}<E$. Correspondingly, $\Psi^{(B)}{}_{JMp}(E^B;\boldsymbol{r},\boldsymbol{R})$ denotes the bound state function.

A. Applying the close-coupling (CC) approach

As characteristic of this approach, the dependence of the scattering and bound state functions on the coordinate R is treated differently than the dependence on the remaining, so-called internal coordinates. First, a number of appropriate basis functions is chosen to represent the dependence on the internal coordinates, denoted here collectively with y. Then, appropriate boundary-value problems for systems of coupled differential equations are formulated whose solutions give the dependence on the R coordinate. The following two bases $\underset{1\times N}{\boldsymbol{\Phi}}{}^{JMp}(y):=\{\Phi_1^{JMp}(y),\ldots,\Phi_N^{JMp}(y)\}$ are particularly useful:

(1) ${}_{\rm SF}\boldsymbol{\Phi}^{JMp}$—expressed in the SF Jacobi coordinates $y=(r,\hat{\boldsymbol{r}},\hat{\boldsymbol{R}})$

$${}_{\rm SF}\Phi_f^{JMp}(r,\boldsymbol{\chi},\hat{\boldsymbol{R}})=\frac{1}{r}\chi_{(vj)_f}(r)\mathcal{Y}_{(jl)_f}^{JMp}(\hat{\boldsymbol{r}},\hat{\boldsymbol{R}}), \tag{18}$$

where $\mathcal{Y}_{jl}^{JMp}(\hat{\boldsymbol{r}},\hat{\boldsymbol{R}})$ is the eigenfunction of the angular momenta operators $\boldsymbol{J}^2$, J_z, $\boldsymbol{j}^2$, and $\boldsymbol{l}^2$

$$\mathcal{Y}_{jl}^{JMp}(\hat{\boldsymbol{r}},\hat{\boldsymbol{R}})=\sum_{m_j,m_l}C(jlJ,m_jm_lM)Y_{jm_j}(\hat{\boldsymbol{r}})Y_{lm_l}(\hat{\boldsymbol{R}}) \quad \text{with } (-1)^{j+l}=p(-1)^J, \tag{19}$$

and $\chi_{vj}(r)$ is the radial rovibrational function of the H_2^+ molecule;

(2) ${}_{\rm BF}\boldsymbol{\Phi}^{JMp}$—expressed in the coordinates $y=(r,\hat{\boldsymbol{r}}_B,\hat{\boldsymbol{R}})$ with $\hat{\boldsymbol{r}}_{\rm B}:=(\theta,\psi)$ and $\theta=\cos^{-1}\hat{\boldsymbol{r}}\cdot\hat{\boldsymbol{R}}$ which are associated with the (two-angle[39]) body-fixed (BF) reference frame having the X, Y, and Z-axes directed along the spherical basis vectors $\mathbf{e}_{\theta_R}$, $\mathbf{e}_{\phi_R}$, and $\mathbf{e}_R:=\hat{\boldsymbol{R}}$, respectively. ψ is the azimuthal angle of the vector $\boldsymbol{r}$ in this frame

$${}_{\rm BF}\Phi_f^{JMp}(r,\hat{\boldsymbol{r}}_B,\hat{\boldsymbol{R}})=\frac{1}{r}\chi_{(vj)_f}(r)\Theta_{(j\lambda)_f}^{JMp}(\hat{\boldsymbol{r}}_{\rm B},\hat{\boldsymbol{R}}), \tag{20}$$

where $\Theta_{j\lambda}^{JMp}(\hat{\boldsymbol{r}}_{\rm B},\hat{\boldsymbol{R}})$ is the parity adapted BF angular function, cf. Ref. 25

$$\Theta_{j\lambda}^{JMp}(\hat{\boldsymbol{r}}_{\rm B},\hat{\boldsymbol{R}})=t_\lambda[(2J+1)/4\pi]^{1/2} \times[D_{M\lambda}^{J*}(\phi_R,\theta_R,0)Y_{j\lambda}(\theta,\psi) + pD_{M-\lambda}^{J*}(\phi_R,\theta_R,0)Y_{j-\lambda}(\theta,\psi)],$$

the index λ, ranging from $\lambda_{\min}(p)=(1-p)/2$ for $p=1$, -1 to $\lambda_{\max}:=\min(J,j)$, is the absolute value of the quantum number associated with the projection of the total angular momentum on the Z axis, $D_{M\lambda}^J(\phi_R,\theta_R,0)$ is an element of the rotation matrix, defined as in Ref. 24, and the factor t_λ equals 1/2 for $\lambda=0$ and $1/\sqrt{2}$ for $\lambda>0$.

Obviously, both bases are orthonormal with respect to the scalar product $[X|Y]:=\int dy X^\dagger(y)Y(y)$ with $\int dy := \int r^2dr\int d\hat{\boldsymbol{r}}\int d\hat{\boldsymbol{R}}$, $d\hat{\boldsymbol{R}}:=d\phi_R d\theta_R\sin(\theta_R)$, and $d\hat{\boldsymbol{r}}$ (or $d\hat{\boldsymbol{r}}_B$) being defined analogously, and are related by an orthogonal matrix $\boldsymbol{U}^{Jp}$

$${}_{\rm SF}\boldsymbol{\Phi}^{JMp}={}_{\rm BF}\boldsymbol{\Phi}^{JMp}\boldsymbol{U}^{Jp}, \tag{21}$$

whose elements are: $[\boldsymbol{U}^{Jp}]_{vj\lambda,v'j'l}=\delta_{v,v'}\delta_{j,j'}[\boldsymbol{U}^{Jp}(j)]_{\lambda l}$ and

$$[\boldsymbol{U}^{Jp}(j)]_{\lambda l}:=U_{\lambda l}^{Jp}(j) = \sqrt{\frac{2}{1+\delta_{0,\lambda}}}(-1)^{J+\lambda}(2l+1)^{1/2}\begin{pmatrix} J & j & l \\ \lambda & -\lambda & 0\end{pmatrix}, \tag{22}$$

for $\lambda=\lambda_{\min}(p),\lambda_{\min}+1,\ldots,\lambda_{\max}$ and $l=|J-j|+\lambda_{\min}$, $|J-j|+\lambda_{\min}+2,\ldots,J+j-\lambda_{\min}$.

Expansions of the scattering functions $\boldsymbol{\Psi}^{(+)}{}_{JMp}(E;\boldsymbol{r},\boldsymbol{R})$ in the two bases yield radial functions ${}_{\rm SF}F_{\alpha_f}^{(+)}{}_{Jp}(E,\alpha_i;R)$ and ${}_{\rm BF}F_{\beta_f}^{(+)}{}_{Jp}(E,\beta_i;R)$, $\beta:=(vj\lambda)$, with $f=1,\ldots,N$ and $i=1,\ldots,N_{\rm o}$, which are collected here in the matrices ${}_{\rm SF}\underset{N\times N_{\rm o}}{\boldsymbol{F}}{}^{(+)}{}_{Jp}(E;R)$ and ${}_{\rm BF}\underset{N\times N_{\rm o}}{\boldsymbol{F}}{}^{(+)}{}_{Jp}(E;R)$, respectively. The radial functions satisfy the coupled equations

$$\left\{\boldsymbol{I}\frac{d^2}{dR^2}+\boldsymbol{k}^{Jp}(E)-\frac{1}{R^2}{}_{\rm fr}\boldsymbol{C}^{Jp}+{}_{\rm fr}\boldsymbol{V}^{Jp}(R)\right\}{}_{\rm fr}\boldsymbol{F}^{(+)}{}_{Jp}(E;R)=0 \quad \text{for fr=SF, BF;} \tag{23}$$

$\boldsymbol{I}$ denotes $N\times N$ unit matrix. The matrices $\boldsymbol{k}^{Jp}$ and ${}_{\rm fr}\boldsymbol{C}^{Jp}$ are diagonal in the channel indices

$$[\boldsymbol{k}^{Jp}]_{vj,v'j'}=\delta_{v,v'}\delta_{j,j'}k_{vj}^2\boldsymbol{I}^{Jp}(j), \tag{24}$$

$$[{}_{\rm SF}\boldsymbol{C}^{Jp}]_{vj,v'j'}=\delta_{v,v'}\delta_{j,j'}\boldsymbol{l}^{Jp}(j), \tag{25}$$

$$[{}_{\rm BF}\boldsymbol{C}^{Jp}]_{vj,v'j'}=\delta_{v,v'}\delta_{j,j'}\boldsymbol{c}^{Jp}(j), \tag{26}$$

$\boldsymbol{I}^{Jp}(j)$ denotes $n\times n$ unit matrix with $n(J,p,j)=\min(J,j)+(1+p)/2$, $\underset{n\times n}{\boldsymbol{l}}{}^{Jp}(j)$ is the diagonal matrix with the elements $l(l+1)$ for l ranging as described in Eq. (22), and $\underset{n\times n}{\boldsymbol{c}}{}^{Jp}(j)$ is the following tridiagonal matrix:

$$[\boldsymbol{c}^{Jp}(l)]_{\lambda,\lambda'}=\delta_{\lambda,\lambda'}[J(J+1)+j(j+1)-2\lambda^2]+\delta_{\lambda',\lambda\pm1}[(1+\delta_{\lambda',0})(1+\delta_{\lambda,0})]^{1/2}\times[J(J+1)-\lambda(\lambda\pm1)]^{1/2}\times[j(j+1)-\lambda(\lambda\pm1)]^{1/2}.$$

Obviously, the following relation takes place:

$$[\boldsymbol{U}^{Jp}(j)]^T\boldsymbol{c}^{Jp}(j)\boldsymbol{U}^{Jp}(j)=\boldsymbol{l}^{Jp}. \tag{27}$$

The matrices ${}_{\mathrm{fr}}\boldsymbol{V}^{Jp}(R)$ in both the SF and BF formulations introduce coupling between different (vj) channels. Elements of ${}_{\mathrm{BF}}\boldsymbol{V}^{Jp}(R)$ are

$$[{}_{\mathrm{BF}}\boldsymbol{V}^{Jp}(R)]_{\beta,\beta'}=\frac{2\mu}{\hbar^2}\sum_L\langle\chi_{vj}|V_L(r,R)\chi_{v'j'}\rangle_r\langle\Theta^{JMp}_{j\lambda}|P_L(\cos\theta)\Theta^{JMp}_{j'\lambda'}\rangle, \tag{28}$$

where P_L for $L=0,2,\ldots$ denote Legendre polynomials and $V_L(r,R)$ come from expansion of the interaction potential $\overline{V}(r,R,\theta)$ into these polynomials; cf. Eq. (39). In the analogous formula for $[{}_{\mathrm{SF}}\boldsymbol{V}^{Jp}(R)]_{\alpha,\alpha'}$, the angular integrals $\langle\Theta^{JMp}_{j\lambda}|P_L(\cos\theta)\Theta^{JMp}_{j'\lambda'}\rangle$ are replaced with Percival–Seaton coefficients $\langle\mathcal{Y}^{Jp}_{jl}|P_L(\cos\theta)\mathcal{Y}^{Jp}_{j'l'}\rangle$.

The conditions obeyed by the radial functions ${}_{\mathrm{SF}}\boldsymbol{F}^{(+)Jp}(E;R)$ are as follows:

$${}_{\mathrm{SF}}\boldsymbol{F}^{(+)Jp}(E;R)\xrightarrow[R\to0]{}0\boldsymbol{I}, \tag{29}$$

$${}_{\mathrm{SF}}\boldsymbol{F}^{(+)Jp}_{\mathrm{o}}(E;R)\xrightarrow[R\to\infty]{}\boldsymbol{O}^{-Jp}(E;R)-\boldsymbol{O}^{+Jp}(E;R)\boldsymbol{S}^{Jp}(E), \tag{30}$$

where the subscript "o" serves to denote the part of the matrix ${}_{\mathrm{SF}}\boldsymbol{F}^{(+)Jp}(E;R)$ that includes the functions ${}_{\mathrm{SF}}F^{(+)Jp}_{\alpha}(E,\alpha_i;R)$ with α corresponding to an open channel, $\boldsymbol{S}^{Jp}$ is the partial scattering matrix, and $\underset{N_o\times N_o}{\boldsymbol{O}}{}^{sJp}(E;R)$ with $s=+,-$ denote diagonal matrices of the respective solutions of the SF coupled equations in the asymptotic region (where the potential coupling vanishes)

$$[\boldsymbol{O}^{\pm Jp}(E;R)]_{\alpha,\alpha_i}=\delta_{v,v_i}\delta_{j,j_i}\delta_{l,l_i}i\sqrt{\frac{\mu}{2\pi\hbar^2}}k_{vj}^{-1/2}\mathcal{H}_l^{\pm}(k_{vj}R), \tag{31}$$

with $\mathcal{H}_l^{\pm}$ being the spherical Ricatti–Hankel functions of lth order, $\mathcal{H}_l^{\pm}(z)\xrightarrow[z\to\infty]{}\exp[\pm i(z-l\pi/2])$. For α corresponding to a closed channel, the function ${}_{\mathrm{SF}}F^{(+)Jp}_{\alpha}(E,\alpha_i;R)$ decays asymptotically like $\mathcal{H}_l^{+}(i|k_{vj}|R)$. The boundary conditions obeyed by the BF radial functions are consistent with the relation

$${}_{\mathrm{BF}}\boldsymbol{F}^{(+)Jp}(E;R)=\boldsymbol{U}^{Jp}\,{}_{\mathrm{SF}}\boldsymbol{F}^{(+)Jp}(E;R)\boldsymbol{U}^{JpT}. \tag{32}$$

Expansion of the bound state function $\Psi^{(B)JMp}(E^B;\boldsymbol{r},\boldsymbol{R})$ in the bases ${}_{\mathrm{fr}}\boldsymbol{\Phi}^{JMp}$ for fr=SF, BF, gives vectors of radial functions $\underset{N\times1}{{}_{\mathrm{fr}}\boldsymbol{F}}{}^{(B)Jp}(E^B;R)$ which satisfy Eq. (23) and the boundary conditions: ${}_{\mathrm{fr}}\boldsymbol{F}^{(B)Jp}(E^B;0)=0$ and ${}_{\mathrm{fr}}\boldsymbol{F}^{(B)Jp}(E^B;R)\xrightarrow[R\to\infty]{}0$.

Finally, the phototransition amplitudes can be written in terms of the radial integrals

$$\boldsymbol{T}_{\mathrm{B}\leftrightarrow\mathrm{F}}(E^BJ^Bp^B;EJp)=({}_{\mathrm{BF}}\boldsymbol{F}^{(B)J^Bp^B}(E^B)|{}_{\mathrm{BF}}\boldsymbol{d}^{J^Bp^BJp}\,{}_{\mathrm{BF}}\boldsymbol{F}^{(+)Jp}(E))\boldsymbol{U}^{Jp}, \tag{33}$$

where $(X|Y):=\int dR X^{\dagger}(R)Y(R)$ and the matrix ${}_{\mathrm{BF}}\boldsymbol{d}^{J^Bp^BJp}$ is built of the following elements:

$$[{}_{\mathrm{BF}}\boldsymbol{d}^{J^Bp^BJp}(R)]_{\beta',\beta}=\frac{4\pi}{\sqrt{3}}\sum_{L,\Lambda}\langle\chi_{v'j'}|d^{\mathrm{BF}}_{L\Lambda}(r,R)\,\chi_{vj}\rangle_r\langle j'\lambda'J^Bp^B\|\Theta^1_{L\Lambda}\|j\lambda Jp\rangle, \tag{34}$$

in which $d^{\mathrm{BF}}_{L\Lambda}(r,R)$ denotes radial component of the dipole moment vector field in the BF angular basis

$$d_{\mu}(\boldsymbol{r},\boldsymbol{R})=\frac{4\pi}{\sqrt{3}}\sum_{L,\Lambda}d^{\mathrm{BF}}_{L\Lambda}(r,R)\Theta^{1\mu1}_{L\Lambda}(\hat{\boldsymbol{r}}_B,\hat{\boldsymbol{R}}), \tag{35}$$

and the reduced matrix element $\langle\|\|\rangle$ is defined consistently with Eq. (8), *viz.* $\langle j'\lambda'J'p'\|\Theta^1_{L\Lambda}\|j\lambda Jp\rangle:=\sqrt{2J'+1}\langle\Theta^{J'M'p'}_{j'\lambda'}|\Theta^{1\mu1}_{L\Lambda}|\Theta^{JMp}_{j\lambda}\rangle/C(J1J',M\mu M')/\sqrt{2J+1}$. Formula for $\langle\Theta^{J'M'p'}_{j'\lambda'}|\Theta^{1\mu1}_{L\Lambda}|\Theta^{JMp}_{j\lambda}\rangle$ in terms of $3j$-coefficients can be found, e.g., in Ref. 25.

B. Dimensionality reducing approximation

When applying the CC approach to evaluate the phototransition amplitudes for the HeH_2^+ system, the calculations can be highly facilitated if part of the Coriolis coupling terms in the BF coupled equations is neglected. This is done by setting a limit $\tilde{\lambda}_{\max}$ on the values of the quantum number λ. The matrices $\boldsymbol{c}^{Jp}(j)$ become reduced to their submatrices of dimension $\tilde{n}:=\min(j,J,\tilde{\lambda}_{\max})+(1+p)/2$, denoted below by $\tilde{\boldsymbol{c}}^{Jp}(j,\tilde{\lambda}_{\max})$. Correspondingly, the potential coupling matrix ${}_{\mathrm{BF}}\boldsymbol{V}^{Jp}(R)$ is reduced by dropping its blocks numbered with $\lambda>\tilde{\lambda}_{\max}$. Respective columns and rows are deleted also from the matrix ${}_{\mathrm{BF}}\boldsymbol{d}^{J^Bp^BJp}(R)$. The reduction affects, of course, the behavior of the resulting approximate radial functions ${}_{\mathrm{BF}}\tilde{\boldsymbol{F}}^{(+)Jp}(E;R)$ in the asymptotic region and all the relations between the corresponding quantities in the BF and SF representations. In particular, the relation (27) is no longer valid for $\boldsymbol{U}^{Jp}$ given by Eq. (22). Diagonalizing the matrix $\tilde{\boldsymbol{c}}^{Jp}(j,\tilde{\lambda}_{\max})$

$$[\tilde{\boldsymbol{U}}^{Jp}(j,\tilde{\lambda}_{\max})]^T\tilde{\boldsymbol{c}}^{Jp}(j,\tilde{\lambda}_{\max})\tilde{\boldsymbol{U}}^{Jp}(j,\tilde{\lambda}_{\max})=\tilde{\boldsymbol{l}}^{Jp}, \tag{36}$$

one obtains eigenvalues $[\tilde{\boldsymbol{l}}^{Jp}]_{i,i}=\eta_i^2-\frac{1}{4}$ for $i=1,\ldots,\tilde{n}$, with η_i differing from half-integer numbers $l_i+(1/2)$ when $\tilde{\lambda}_{\max}$ is smaller than both j and J. The corresponding approximate functions ${}_{\mathrm{SF}}\tilde{\boldsymbol{F}}^{(+)Jp}(E;R)$ can be introduced as

$\tilde{\boldsymbol{U}}^{Jp\,T}(\tilde{\lambda}_{\max})\,{}_{\rm BF}\tilde{\boldsymbol{F}}^{(+)_{Jp}}(E;R)\tilde{\boldsymbol{U}}^{Jp}(\tilde{\lambda}_{\max})$ using transformation $\tilde{\boldsymbol{U}}^{Jp}(\tilde{\lambda}_{\max})$ built of appropriate matrices $\tilde{\boldsymbol{U}}^{Jp}(j,\tilde{\lambda}_{\max})$. From the relations given above, it is obvious how one could construct the corresponding reduced representations of the intermolecular potential and of the dipole moment in the SF frame. These quantities are not needed, however. The reduced BF coupled equations can be used for numerical generation of the radial functions. The transformation to the SF frame serves only imposition of appropriate asymptotic form on the functions generated; it needs to be done only once, in the region where the potential coupling vanishes. Obtaining the necessary formula for the functions ${}_{\rm SF}\tilde{\boldsymbol{F}}^{(+)_{Jp}}(E;R)$ in the asymptotic region is only a matter of redefining the matrices $\boldsymbol{O}^{\pm Jp}$ in Eq. (30). Namely, the spherical Ricatti–Hankel functions $\mathcal{H}_l^s(k_{vj}R)$ for $s=+,-$ have to be replaced in Eq. (31) with the Hankel functions of appropriate real order η, strictly with $i\sqrt{\pi/2}(k_{vj}R)^{1/2}H_\eta^{(k)}(k_{vj}R)$ for $k=1,2$, respectively, where k denotes the kind of Hankel function.

V. DETERMINATION OF RESONANCE CHARACTERISTICS

Information on the resonance positions and widths, $E^{\rm res}$ and Γ, is contained in the (excess) continuum density of states $\Delta\rho^{Jp}(E)$, which is known[40,27] to be directly related to the collision time-delay matrix $\boldsymbol{Q}^{Jp}(E)$,[41]

$$\Delta\rho^{Jp}(E)=\frac{1}{2\pi\hbar}\,{\rm Tr}\boldsymbol{Q}^{Jp}(E),$$

where

$$\boldsymbol{Q}^{Jp}(E)=i\hbar\,\frac{d\boldsymbol{S}^{Jp\dagger}(E)}{dE}\,\boldsymbol{S}^{Jp}(E). \tag{37}$$

A convenient formula for evaluation of the matrix $\boldsymbol{Q}^{Jp}$ within the CC approach (avoiding numerical differentiation of the $\boldsymbol{S}^{Jp}$ matrices), as well as a procedure of extraction of the required information on resonances, are described in Ref. 42.

As to determination of the radiative widths, $\Gamma_{\rm rad}$, the description of Sec. III needs to be supplemented with a specification of the Q subspace which supports the resonances of interest. Since they are in majority shape resonances, the Q subspace is most appropriately chosen as a confined part of the configuration space available to the atom–diatom system so-called interaction region, bounded by a surface $R=R_\infty$, where R_∞ is large enough for $\boldsymbol{V}^{Jp}(R_\infty)\approx 0$. This choice is characteristic of the R-matrix theory of resonances.[36] Following the well-known procedures of this theory, the state $\langle \boldsymbol{r},\boldsymbol{R}|E^{B_Q}JMp\rangle_Q$, strictly the radial functions $\boldsymbol{F}_Q^{(B)_{Jp}}(R)$ representing this state in the basis ${}_{\rm BF}\tilde{\boldsymbol{\Phi}}^{JMp}$ (the tilde denotes possible reduction of dimensionality of the basis) can be found as a solution to the eigenvalue problem

$$[E\boldsymbol{I}-\boldsymbol{H}^{Jp}(R)-\boldsymbol{B}(R;R_\infty)]\boldsymbol{F}_Q^{(B)_{Jp}}(R)=0\boldsymbol{I}, \tag{38}$$

where $\boldsymbol{H}^{Jp}(R):=R[{}_{\rm BF}\tilde{\boldsymbol{\Phi}}^{JMp}|H(1/R)\,{}_{\rm BF}\tilde{\boldsymbol{\Phi}}^{JMp}]$ and $\boldsymbol{B}(R;R_\infty):=(\hbar^2/2\mu)\,\delta(R-R_\infty)\boldsymbol{I}(d/dR)$ is (a version of) the Bloch boundary condition operator. Since the functions $\boldsymbol{F}_Q^{(B)_{Jp}}(R)$ are needed only for evaluation of the radiative widths of sharp resonances, and functions pertaining to such resonances should have very small amplitudes outside the interaction region, there is some freedom to modify the above eigenvalue problem without a danger of introducing any major difference (error). In particular, one can use the boundary condition operator $\boldsymbol{B}^\dagger$ instead of $\boldsymbol{B}$ which means practically that functions with zero values at the R_∞ boundary are to be generated instead of functions having specified (zero) derivatives at this boundary.

VI. CALCULATIONS

A. Electronic structure input

Both the intermolecular potential $\overline{V}(r,R,\cos\theta)$ and the diatomic potential $V_{\rm HH^+}(r)$ were extracted from the analytical fit to the *ab initio* potential energy surface (PES) for the ground electronic state of the HeH_2^+ system, published in Ref. 15

$$V(r,R,\cos\theta)=\sum_L V_L(r,R)P_L(\cos\theta)$$

$$=\overline{V}(r,R,\cos\theta)+V_{\rm HH^+}(r). \tag{39}$$

The parameters of the fit are constrained to give $\lim_{R\to\infty}V_{L>0}(r,R)=0$, and

$$V_{\rm HH^+}(r):=\lim_{R\to\infty}V_0(r,R). \tag{40}$$

The necessary dipole moment functions $d_{L\Lambda}^{\rm BF}(r,R)$, for $\Lambda=0,1$ and for L, assuming even values ($L\geqslant 2\Lambda$), are directly related to the functions $D_{L\Lambda}(r,R)$

$$d_{L\Lambda}^{\rm BF}(r,R)=\frac{1}{\sqrt{2L+1}}\sqrt{\frac{(L+\Lambda)!}{(L-\Lambda)!}}D_{L\Lambda}(r,R), \tag{41}$$

which arise from the following expansions of the components $d_Z(\boldsymbol{r},\boldsymbol{R})=d_0^{\rm BF}(\boldsymbol{r},\boldsymbol{R})$ and $d_{\tilde{X}}(\boldsymbol{r},\boldsymbol{R})=-(1/\sqrt{2})\,d_1^{\rm BF}(\boldsymbol{r},\boldsymbol{R})$ ($d_{\tilde{Y}}=0$) of the dipole moment vector in the $\tilde{X}\tilde{Y}Z$ reference frame, in which the spherical and azimuthal angles of the vectors $\boldsymbol{R}$ and $\boldsymbol{r}$ are (0,0) and (θ,0), respectively, cf. Ref. 43

$$(-1)^\Lambda\sqrt{1+\Lambda}\,d_\Lambda^{\rm BF}(r,R,\theta)=\sum_L D_{L\Lambda}(r,R)P_L^\Lambda(\cos\theta); \tag{42}$$

P_L^Λ denotes here the associated Legendre function. The functions $D_{L\Lambda}(r,R)$ were determined in Ref. 44 by fitting to *ab initio* calculated data for the dipole moment. Actually, only the d_Z component of the dipole moment vector was accounted for in the calculations of this work.

B. Some details on CC equations

The coupled equations for the $He+H_2^+(I)$ system were constructed using functions of 32 rovibrational states of H_2^+: with $v=0,1,2,3$ and $j=0,2,\ldots,14$ for $I=0$ and $j=1,3,\ldots,15$ for $I=1$. The radial functions of the states, $\chi_{vj}(r)$, were generated from the potential (40). The energies ε_{vj} obtained for the lowest ($v=0j$) states are, respectively, 58.22, 174.20, 347.02 $\rm cm^{-1}$ for $j=1,2,3$ (these energies are relative to the dissociation limit $\varepsilon_{v=0\,j=0}$). The choice of the rovibrational

TABLE I. Count of the functions $[\partial R^I(\mathcal{B};EJp)/\partial E]$ contributing to the rate constant $k^I(T)$.

Bound states[a]	$\mathcal{B}:=([v],k,J^B,p^B)$ where $[v]:=(v_r,v_\theta,v_R)$												
	$I=0$ (j even)						$I=1$ (j odd)						
	$p^B=1$			$p^B=-1$[b]			$p^B=1$				$p^B=-1$		
	$k=0$	1	2	$k=1$	2	3	$k=0$[c]	1[c]	2	3	$k=1$	2	3
No. of states	103	41	16	67	37	4	106	62	16	2	64	16	2
No. of $[v]$[d]	9	4	2	8	6	1	9	8	2	1	8	2	1
Transitions[e]	$R,P,Q:=J\rightarrow J^B=J+1,-1,+0$												
No. of R,P	311			*208*			363				156		
No. of Q	*151*			*108*			$80+97$[f]				82		

[a]The dissociation limit of f-parity states of HeH_2^+ (*para*) lies 174.20 cm^{-1} above the limit of e states (zero of E). All states of HeH_2^+ (*ortho*) are bound up to $E=58.22$ cm^{-1}.

[b]Fifty-one of the states counted here lie above the dissociation limit of j even-e states.

[c]Assignment of e-parity states with $k=0$ or $k=1$ is ambiguous in some cases.

[d]Groups of levels assigned with the same values of k and p^B and different $[v]$ will be enumerated: $[v]=1,2,\ldots$, according to the position on the energy scale of the lowest ($J^B=k$) levels of the groups, $E([v]=1,k,J^B=k,p^B)<E([v]=2,k,k,p^B)\ldots$.

[e]Italic numbers denote that none of the corresponding functions was determined within the entire energy range 0–300 cm^{-1}. Only sharp resonance structures ($\Gamma<1$ cm^{-1}) occurring in these functions were determined.

[f]Counted are here the Q-transitions to $k=0$ states. They are not directly allowed by the Z component of dipole moment and therefore are weak.

basis was made in calculations of bound state energies of the HeH_2^+ ion for low values of J (i.e., $J\leqslant 2$). The convergence error of the energies with respect to inclusion of functions with higher v or j was smaller than 0.01 cm^{-1}. With the above (v,j) channels included, the number N of the (v,j,l) or (v,j,λ) states coupled in the SF or BF radial equations would grow quickly with J, reaching the value of 288 for $J\geqslant 15$ (j odd and $p=1$). Since many thousands of individual solutions of the CC equations were estimated to be needed for the evaluation of the rate constant (cf. Sec. VI E), the reduction of the dimensionality of the systems of these equations was desirable. Possibilities of such reduction were tested in preparation of every major stage of the calculations, such as the determination of all bound states of the HeH_2^+ ion in the PES used, the determination of parameters of relevant sharp resonances, and the evaluation of free-bound transition amplitudes (cf. the following subsections). The conclusion of the tests was that the parameter $\tilde{\lambda}_{\max}$, controlling the elimination of the Coriolis coupling terms from the BF coupled equations, can be set as small as 4. Thus, the maximal sets of the CC equations solved for e-parity states of $He+H_2^+$ (*ortho*) and $He+H_2^+$ (*para*) systems included 144 and 136 equations, respectively. For f states, the respective maximal dimensions were 112 and 104.

In calculations on bound states of the HeH_2^+ ion, the coupled equations were typically integrated within the range of 1–9 Å. A larger range, extending up to 20 Å, was necessary in calculation of some energies (very) close to the dissociation limits. The bound-type calculations for sharp resonances, Eq. (38), were done with $R_\infty=9$ Å. In calculations concerning continuum states, the integration range was 1–15 Å. The continuum energy range covered in the calculations extended up to 300 cm^{-1} above the dissociation limit. All the CC calculations were carried out with the help of the log-derivative method[45,46] using a step size of 0.02 Å. All the necessary versions of the method (for evaluation of bound-free transition amplitudes, lifetime matrices, bound-state energies and functions) are coded in the computer program exploited previously in the theoretical simulations of the absorption spectrum of the Ar–HD complex.[42,47] For the present task, the program was supplemented with the option for performing the reduced dimensionality calculations.

C. Bound states

Essential features of the rovibrational energy spectrum of the HeH_2^+ ion are well-known from the previous work on the subject.[48–51] The energy levels are usually labeled with the two good quantum numbers J and p and with four approximate quantum numbers, v_r, v_θ, v_R, and k. The v numbers describe the vibrational motions along the indicated coordinates and k correlates with the vibrational angular momentum quantum number of linear molecules; here, it should be identified with the value of the quantum number λ which is dominant in a given state. Because of the need for a dimensionality reducing approximation, the natural question arose how dominant the k number really is in states characterized by higher values of J. If k were a nearly good quantum number, the coupled states (CS) approximation[51] could be applied, i.e., only $\lambda=k$ states could be retained in the BF coupled equations. Unfortunately, energies of the $J>10$ states calculated in this approximation revealed unacceptable errors, exceeding 100 cm^{-1} for the $J=12$- and 200 cm^{-1} for the $J=19$ states. In order to obtain values of these energies with an accuracy within 0.1–0.5 cm^{-1}, the Coriolis coupling between the $\lambda=0$ to $\lambda=4$ states had to be included.

Altogether, 536 bound states are supported by the used PES. Half of them are states of the HeH_2^+ (*para*) ion. The states can be classified into 61 different rovibrational groups

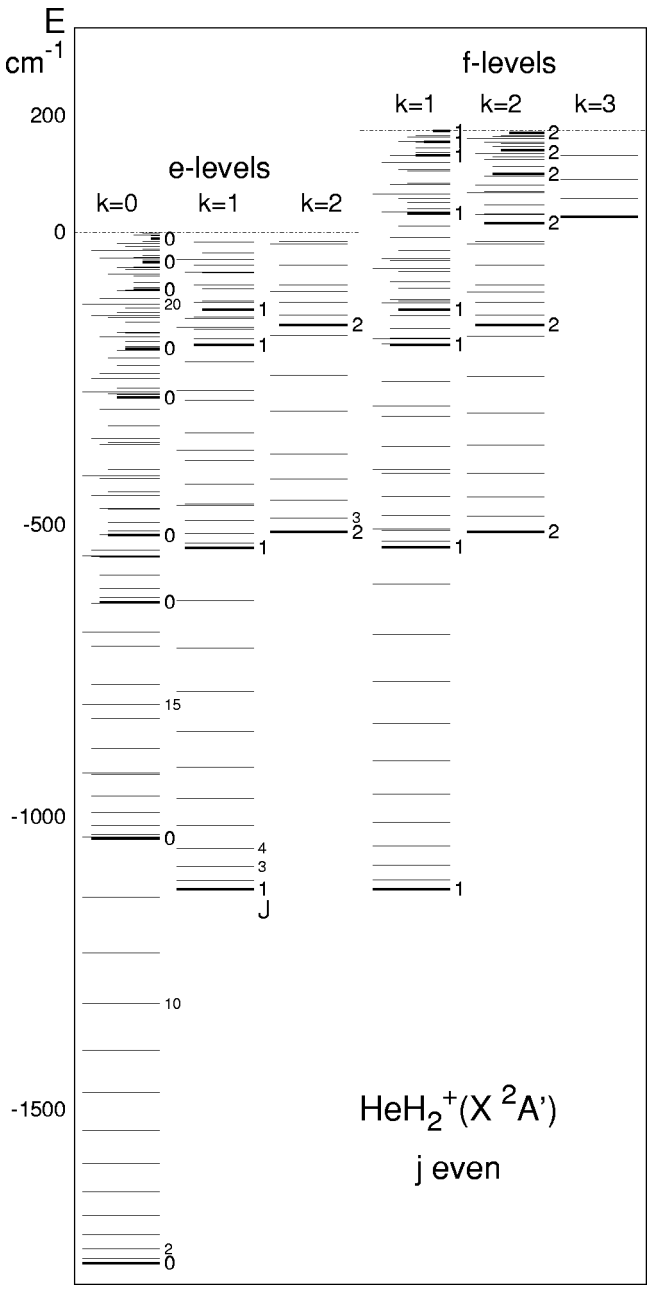

FIG. 1. The spectrum of bound rovibrational states of the HeH_2^+(*para*) ion. The way of presentation of the spectrum in the figure reflects the labeling of the states; cf. Table I. Energies of states characterized with the same p- and k numbers are drawn as one ladder of levels. Thicker lines in a ladder denote levels with $J=k$. They are the lowest levels of different ro-vibrational groups $([v],k,p)$. $J \geqslant k$ levels belonging to different groups within a given (p,k) ladder are distinguished by lengths of the horizontal lines.

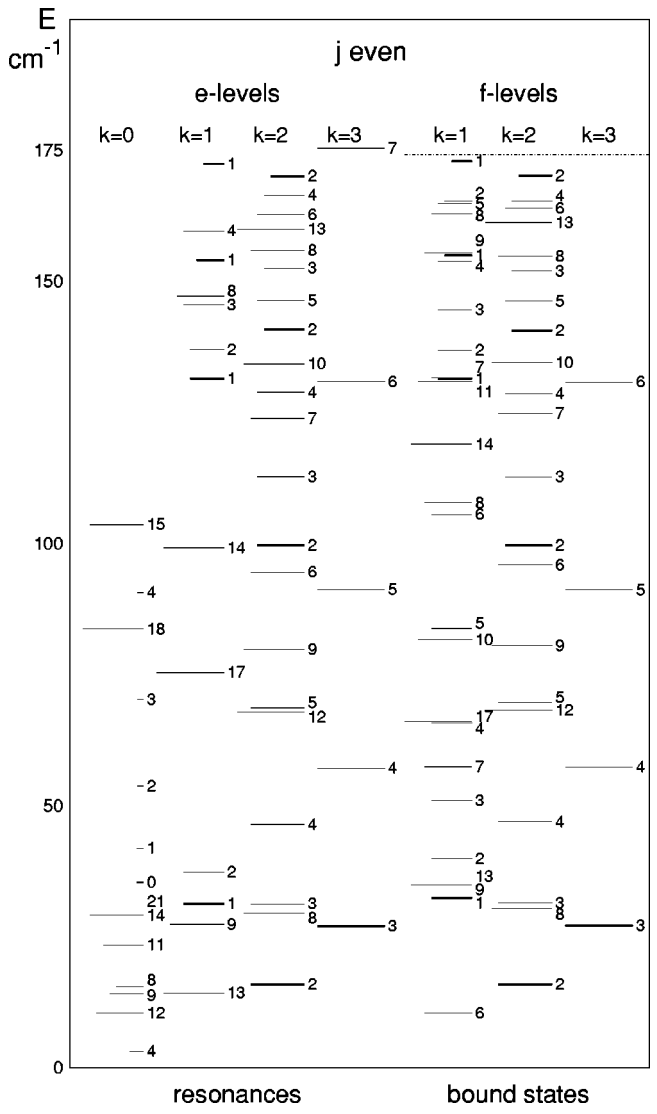

FIG. 2. Energy levels of HeH_2^+(*para*) above the $He+H_2^+(v=0,j=0)$ threshold, in the range up to 175 cm^{-1}. Only resonances whose widths are smaller than 1 cm^{-1} are shown in this figure.

$([v_r,v_\theta,v_R],k,p)$, cf. Table I. The pattern of energy levels is presented in Fig. 1. Though the PES used here is not expected (cf. Ref. 15) to provide rovibrational spectrum of the ion which would be more reliable than that calculated in Refs. 14 and 50, a comparison seems in order. First, one should note that the $k=J=0$ and $k=J=1$ levels (denoted with thicker lines in Fig. 1) form the same pattern as the levels from the Meuwly–Hutson potential shown in Fig. 6 of Ref. 14. The pattern of near-dissociation levels of HeH_2^+(*ortho*) yielded by the potential is also similar (for $J \leqslant 4$) to that presented in Fig. 8 of Ref. 14. Obviously, differences in positions of the individual levels are too big (of order of 0.5–2 cm^{-1}) for a meaningful comparison of transition frequencies in this region. The energies of $J \rightarrow J-1$ rotational transitions in the three lowest vibrational states listed in Table I of Ref. 52 are reproduced by the present potential with deviations of 0.1–0.8 cm^{-1} for $J=1-10$ in the ground state and with deviations of 0.7–5.2 cm^{-1} in the lowest bend $(k=1)$ state.

D. Resonances

Figure 2 shows the spectrum of energy levels of HeH_2^+(*para*) ion in the region up to 175 cm^{-1} above the $He+H_2^+(v=0,j=0)$ threshold. The pattern of f-parity bound-states energies is shown here in more detail than in Fig. 1 and, which is the main purpose, the positions of $\Gamma < 1$ cm^{-1} resonances in this region are demonstrated. The resonance energy levels are drawn and assigned as a continuation of the progression of the e-parity bound-states energy levels. A comparison of positions of the corresponding e-

TABLE II. Convergence with the parameter $\tilde{\lambda}_{max}$ of energies and widths of selected resonances.

p	k	J	$\tilde{\lambda}_{max}$	E^{res} cm^{-1}	Γ cm^{-1}	Γ_{rad}[a] 10^{-11} cm^{-1}	$\Gamma/(\Gamma_{rad}+\Gamma)$
				j even			
1	0	9	3	14.18	2.13 (−03)	4.89	1.00
			4	14.12	2.09 (−03)	4.91	1.00
		11	1	27.63	1.79 (−03)	6.59	1.00
			3	23.47	2.13 (−04)	7.33	1.00
			4	23.44	2.27 (−04)	7.34	1.00
		12	1	34.85	5.66 (−06)	8.64	1.00
			2	14.59	2.62 (−10)	8.11	0.76
			3	10.10	1.00 (−11)	7.83	0.11
			4	10.46	5.00 (−12)	7.73	0.06
		14	1	39.96	3.20 (−07)	12.79	1.00
			3	29.24	2.78 (−09)	13.98	0.95
			4	29.10	2.55 (−09)	13.99	0.95
		18	1	112.36	1.55 (−07)	13.15	1.00
			3	84.15	5.25 (−10)	12.51	0.81
			4	83.71	4.73 (−10)	12.46	0.79
	1	14	3	99.93	2.91 (−03)	4.46	1.00
			4	99.25	3.06 (−03)	4.54	1.00
		17	3	76.42	1.11 (−09)	6.76	0.94
			4	75.46	9.15 (−10)	6.72	0.93
	2	5	3	69.19	5.04 (−02)	3.58	1.00
			4	68.62	3.10 (−02)	3.48	1.00
			5	68.16	3.09 (−02)	3.47	1.00
		8	3	30.56	1.15 (−02)	2.07	1.00
			4	29.59	8.36 (−03)	2.13	1.00
			5	29.56	8.27 (−03)	2.13	1.00
	3	5	3	101.36	6.02 (−02)	2.02	1.00
			4	91.22	2.57 (−02)	2.10	1.00
			5	91.16	2.54 (−02)	2.11	1.00
				j odd			
1	0	13	3	97.40	7.54 (−04)	4.79	1.00
			4	97.02	6.48 (−04)	4.77	1.00
	1	11	3	78.99	3.30 (−06)	4.86	1.00
			4	78.80	3.36 (−06)	4.90	1.00
−1	1	11	3	76.11	5.24 (−06)	3.79	1.00
			4	75.88	4.46 (−06)	3.84	1.00

[a]$\tilde{\lambda}_{max}$ was varied only in the calculations of the functions $\boldsymbol{F}_Q^{(B)Jp}(R)$; cf. Eq. (38). The bound-state functions in the transition amplitudes $T(\mathcal{B};E^{B_Q}Jp)$; cf. Eq. (16)–(17), were in all cases determined with $\tilde{\lambda}_{max}=4$.

and f levels from the $k=1$ ladders, in particular those assigned with large J numbers, gives further evidence of a significant Coriolis coupling in the system. The observed shifts between the levels are due to the fact that f-parity $k=0$ states do not exist and therefore the $k\geqslant 1$ states are subject to fewer couplings than their e-parity counterparts.

A more detailed presentation of the effect of the Coriolis coupling on resonances, not only on their positions but also on the widths, is given in Table II. One can see that including enough Coriolis coupling terms (i.e., using $\tilde{\lambda}_{max}$ sufficiently larger than the k numbers characterizing the resonances) is particularly important for obtaining convergent widths Γ, especially the very small ones. The radiative widths reveal much less sensitivity to the accuracy of the resonance functions; this seems to be associated with the character of the formula describing these widths (i.e., the matter–radiation interaction is treated in first order). Fortunately, the radiative widths are the more crucial characteristics of resonances for the purpose of evaluation of the association rate constant; cf. Eq. (13). The explicit involvement of the nonradiative widths is through the sharp resonance cutting factor in Eq. (13). As demonstrated in the last column of Table II, sensitivity of this factor to the Coriolis coupling controlling parameter $\tilde{\lambda}_{max}$ is again definitely smaller than the sensitivity of the widths Γ themselves.

There are 53 "nonbroad" ($\Gamma<1\ cm^{-1}$) resonances of the $HeH_2^+(para)$ ion in the energy range shown in Fig. 2. For $HeH_2^+(ortho)$, 23 such resonances were found in the same range (strictly, in $58.22-175\ cm^{-1}$). As it follows from Eq. (13), contribution of a given resonance to the rate constant $k(T)$ is the larger the larger is $(2J+1)\Gamma_{rad}$ (provided the inequality $\Gamma_{rad}\ll\Gamma$ holds) and the smaller is E^{res}. The most contributive resonances are listed in Table III. Shown also are all the cases encountered in which the factor $\Gamma/(\Gamma_{rad}+\Gamma)$ became operative.

E. Free-bound and resonance-bound transitions

There are as many as 1556 functions $[\partial R^I(\mathcal{B};EJp)]/\partial E$ which describe all the allowed transitions to the 536 bound

TABLE III. Energies and widths, nonradiative and radiative (all in cm^{-1}), of some important resonances.

p	k	$[v]$[a]	J	E^{res}	Γ	$\Gamma_{rad}\times 10^{11}$	$\Gamma/(\Gamma_{rad}+\Gamma)$
				j even			
1	0	7	8	15.4	3.4 (−01)	4.5	1
		6	9	14.1	2.1 (−03)	4.9	1
		5	11	23.4	2.3 (−04)	7.3	1
		4	12	10.5	5.0 (−12)	7.7	0.06
		3	14	29.1	2.6 (−09)	14.0	0.95
		3	15	103.7	1.5 (−02)	10.6	1
		2	18	83.7	4.7 (−10)	12.5	0.79
		1	21	31.7	~0[b]	5.5	0
	1	3	9	27.4	5.5 (−01)	4.8	1
		2	13	14.3	~0[b]	6.2	0
		2	14	99.2	3.1 (−03)	4.5	1
		1	17	75.5	9.1 (−10)	6.7	0.93
	2	2	8	29.6	8.4 (−03)	2.1	1
		2	9	79.8	1.6 (−01)	1.5	1
		1	12	67.9	1.1 (−01)	3.2	1
				j odd			
1	0	7	8	66.4	6.4 (−03)	3.2	1
		5	12	91.3	1.8 (−02)	8.0	1
		4	13	97.0	6.5 (−04)	4.8	1
		3	15	103.8	3.3 (−06)	12.3	1
		2	18	83.6	~0[b]	12.4	0
	1	3	11	78.8	3.4 (−06)	4.9	1
		2	14	102.7	2.4 (−05)	6.2	1
		1	17	75.5	~0[b]	6.7	0
	2	2	8	79.5	9.5 (−02)	5.1	1
		1	12	67.9	9.2 (−11)	3.1	0.75
−1	1	3	11	75.9	4.5 (−06)	3.8	1
		2	14	115.3	1.4 (−05)	6.9	1
		1	17	66.0	~0[b]	3.9	0
	2	2	8	76.8	4.5 (−01)	3.4	1
		1	12	67.9	~0[b]	3.2	0

[a]The enumeration of the rovibrational groups of bound-state energy levels is continued for the quasibound levels, so the meaning of $[v]$ numbers is here the same as explained in Table I.
[b]Γ much smaller than the corresponding Γ_{rad}; the resonance does not participate in the association process.

states of HeH_2^+; cf. Table I. If the association rate constant $k(T)$ at low temperatures, below 100 K, say, is of interest, the functions should be (possibly accurately) known at low energies E, in the range extending up to ca. 300 cm^{-1} above the dissociation threshold (at $E=0$). There are many resonances in this range whose widths vary by several orders of magnitude, from $\Gamma\approx 10$ cm^{-1} to $\Gamma\ll 10^{-9}$ cm^{-1}. Although the sharpest resonances can (and even should) be treated separately, as described above, the functions $[\partial R^I(\mathcal{B};EJp)]/\partial E$ still have to be known on a rather dense and highly nonuniform grid of energy points; see Fig. 3 for examples of the functions $[\partial R^I(\mathcal{B};EJp)]/\partial E$ and for a demonstration of their sensitivity to the Coriolis coupling. Thus, determination of all the free-bound transition amplitudes involved would be a formidable computational task. Fortunately, considerable savings become possible if one makes an estimation of the contributions brought by the various amplitudes to the rate constant. In the first place, accounting for resonances of intermediate and larger widths, i.e., not amenable to the treatment of Sec. III, should be considered. Some preliminary tests indicated that resonance-bound transitions may be important even if the terminal states lie not far from the dissociation limit. Therefore, it was decided to include contributions of (possibly) all the resonance structures that appear in all the functions $[\partial R^I(\mathcal{B};EJp)]/\partial E$ due to resonances of widths smaller than 1 cm^{-1}. Altogether, contributions from about 1200 resonance structures in the functions $\partial R^I(\mathcal{B};EJp)$ were actually determined (the extremely sharp ones) are also counted here.

As to contribution of background parts of the functions $[\partial R^I(\mathcal{B};EJp)]/\partial E$, describing direct free-bound transitions (i.e., transitions from continuum regions characterized by smoothly varying density of states), the discriminating factors are: (i) the population factor of initial states, $\exp(-E/k_BT)$, and (ii) the energy released in the transitions, entering as $(E-E^B)^3$ into the formula for the rate constant. The first factor allows one to neglect all the functions for the R and P transitions to f-parity states of HeH_2^+(*para*) (the continuum for these transitions begins at $E=174.20$ cm^{-1}); cf. Table I. Because of the second factor it is possible to eliminate evaluation of (the background parts of) the functions for transitions to highly excited bound states.

In effect of the above estimations, only one-third of the 1536 functions $[\partial R^I(\mathcal{B};EJp)]/\partial E$ was actually determined over the entire energy range specified (0–300 cm^{-1}). On average, the range was covered with 300 points. The spacing between the points was adjusted to the positions of resonances included in the background (all resonances of widths

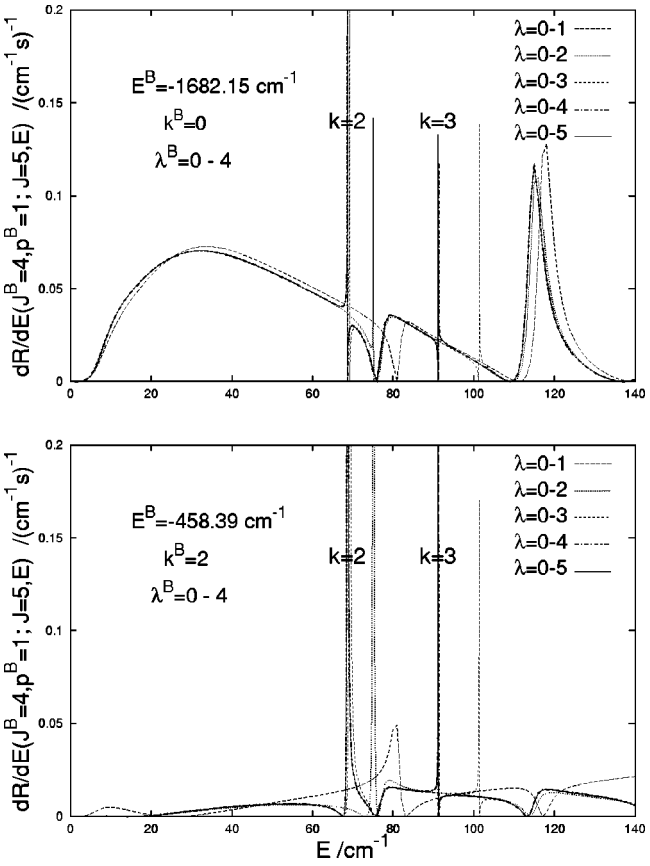

FIG. 3. Exemplary rates $[\partial R^I(\mathcal{B};EJp)]/\partial E$ of association into two different bound states $\mathcal{B}=([v]=1,k^B,J^B=4,p^B=1)$, with $k^B=0$ and $k^B=2$, as functions of energy E of the initial partial continuum state with $J=5$ (the continuous lines). Apart from the two sharp resonances (cf. Table II for their parameters) occurring in both rates, a broad resonance of width $\Gamma \approx 4\ \mathrm{cm}^{-1}$ is seen in the $k^B=0$ case. Convergence of the rates with respect to the number of λ components ($\lambda=0-\tilde{\lambda}_{\max}$) retained in the continuum state is also demonstrated (by proximity of the broken lines to the respective continuous line, representing full CC results). The observations to be made: (i) For accurate determination of the background part of the function $[\partial R^I(\mathcal{B};EJp)]/\partial E$, it would be sufficient if λ components up to k^B+1 were present in the continuum state. (ii) In order to account simultaneously for the structures due to the $k=0-3$ resonances it is safer to keep always the $\lambda=0-4$ components. Hence, the choice of $\tilde{\lambda}_{\max}=4$ was made in all the calculations.

larger than $1\ \mathrm{cm}^{-1}$ and most of the resonances of widths between $0.1-1\ \mathrm{cm}^{-1}$).

VII. RESULTS OF THE RATE CONSTANT CALCULATION

For the rate constant determination, cubic spline interpolations were made between calculated points of the functions $[\partial R^I(\mathcal{B};EJp)]/\partial E$ in order to perform the required integration over energy. Contributions from sharp resonances not included in the background were evaluated using the expression (13).

The results of these calculations obtained for the temperature interval $2 \leqslant T \leqslant 100$ K are collected in Table IV and plotted in Fig. 4. In the upper panel of this figure, the total rate constant for the formation of HeH_2^+ and its decomposition into the HeH_2^+(*para*) and HeH_2^+(*ortho*) formation rate constants [according to the aforementioned expression $k(T)=k^0(T)+k^1(T)$ with 0 and 1 representing the *para*- and *ortho* ions, respectively] are plotted. These individual association rate constants $k^I(T)$ are also displayed separately in the lower two panels, together with their contributions from the most important resonances with $J>7$ and the respective largest constituents leading to the formation of rovibrational levels characterized by the indices $([v],k,p)$ for the two different forms of the ion where the numbering $[v]=1,2,3$ refers to the ordering of the corresponding levels with the lowest $(J=k)$ values in Fig. 1.

TABLE IV. Rate constant k, in $10^{-20}\ \mathrm{cm}^3\ \mathrm{s}^{-1}$, as function of temperature T, in K.

T	k	T	k
2	0.5	26	2.0
6	1.0	28	2.0
8	1.3	30	2.0
10	1.5	40	1.8
12	1.7	50	1.6
14	1.9	60	1.4
16	2.0	70	1.3
18	2.0	80	1.2
20	2.1	90	1.1
22	2.1	100	1.0

The rate constant curve in the upper panel of the figure shows the typical temperature dependence for relatively weakly bound systems. It has a broad maximum of $2.1 \times 10^{-20}\ \mathrm{cm}^3\ \mathrm{s}^{-1}$ around $T=20$ K and a moderately fast fall-off at higher temperatures. In the maximum region the dominating contributions to $k(T)$ arise from j-even levels, whereas the j-odd contributions are slightly more dominating at temperatures above 50 K. Similar temperature functions for the total rate constant have previously been found for atom–atom associations.[17] Actually for the related proton–helium association the maximum rate constant has previously been determined[32,34,35] to be about one order of magnitude larger compared to the present result. Since the rate constant is strongly dependent on the photon energy released in the radiative process, this can in principle be rationalized as a consequence of the large difference between the binding energies of HeH^+ and the triatomic complex, $16\,455\ \mathrm{cm}^{-1}$ as compared to $2703\ \mathrm{cm}^{-1}$ for HeH_2^+. Considering this large energy difference, it appears somewhat surprising though that the rate constants differ only by one order of magnitude. According to some earlier theoretical considerations (Refs. 29, 30 and also Ref. 31) this can, however, be related to the fact that resonance contributions can significantly enhance the radiative association rates at low temperatures. Whereas in HeH^+ essentially only two resonances at low energies were found to drive the association reaction, the present calculations show that in HeH_2^+ a large number of resonances exist which are contributing to the radiative process. The much smaller energy gain in the radiative stabilization of the $He+H_2^+$ association process is thus partly compensated by a larger number of resonance contributions to the rate constant.

For a better understanding of the dynamics of reaction (2), it seems therefore to be helpful to discuss here in more

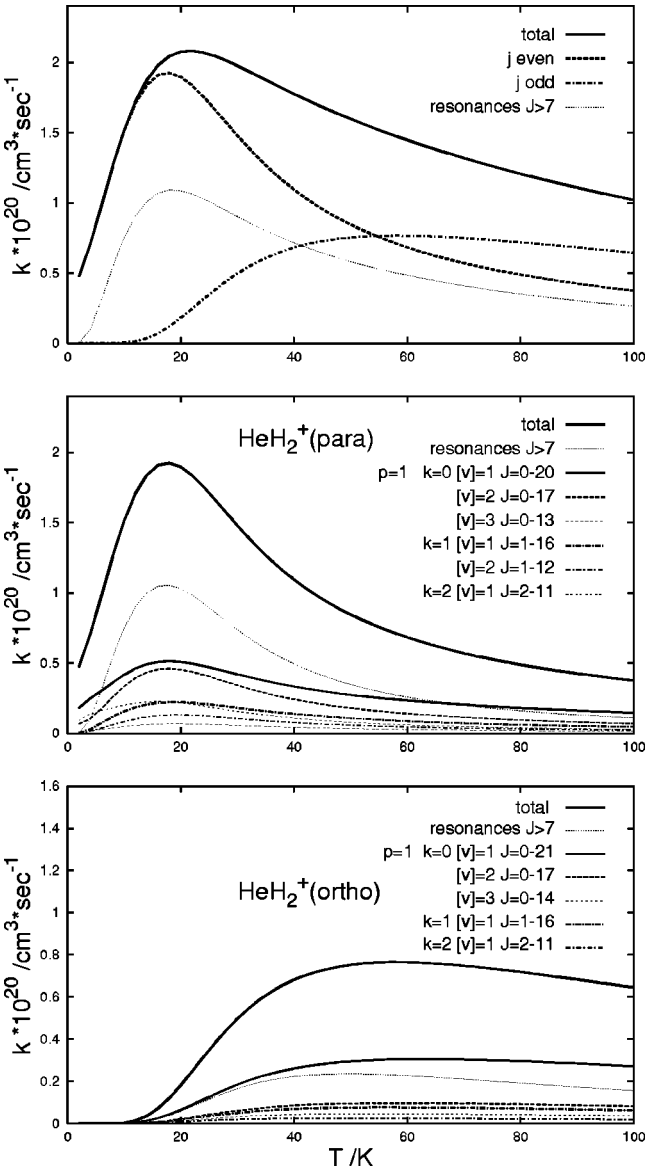

FIG. 4. Upper panel: The rate constant for formation of the HeH_2^+ ion and its decomposition into parts describing formation of the HeH_2^+(*para*) and HeH_2^+(*ortho*) ions. Middle panel: The association rate constant $k^0(T)$, the contribution of the most important resonances (with $J>7$), and the largest constituents of $k^0(T)$ which describe formation of the HeH_2^+(*para*) ion in states belonging to different rovibrational groups ($[v],k,p$). The numbers $[v]=1,2,3...$, give the ordering on the energy scale of the lowest ($J=k$) levels from the groups assigned with the same values of k and p (forming the same ladder in Fig. 1.) Bottom panel: Same for the HeH_2^+(*ortho*) ion.

detail the role of resonances in the formation of the HeH_2^+ ion. Obviously, in contrast to the light HeH^+ ion the density of quasibound and continuum levels above the dissociation threshold is much larger for the triatomic complex. Due to this dense energy level pattern it is very difficult, or rather impossible, to distinguish between resonance-bound and free-bound contributions to $k(T)$. There is in general no clear-cut difference between their widths, and even the magnitudes of the resonance widths themselves change considerably (see Table III). In this situation an attempt was made here to obtain a realistic lower estimate of the total resonance contributions to the total rate constant by summarizing the contributions from sharp resonances with $J>7$ which are more easy to account for separately. In the three panels of Fig. 4 the thick solid curves for the total rate constant are compared with small dotted curves representing these resonance contributions. In the case of the total rate constant in the upper panel, the high-J contributions already account for about 40 percent in the maximum region of the temperature function. It was previously discussed in this paper that sharp resonances are treated by applying the formula (13) of Bain and Bardsley,[31] rederived here in the context of atom–diatom associations. This formula contains the factor $\Gamma/(\Gamma_{\mathrm{rad}}+\Gamma)$ (cutting factor) which is needed to cut out resonances with $\Gamma \ll \Gamma_{\mathrm{rad}}$ that are not in thermal equilibrium and therefore have to be excluded from the summation for the rate constant $k(T)$. If this factor had not been taken into account the maximum of the function $k(T)$ would rise to $3.2 \times 10^{-20}\ \mathrm{cm}^3\ \mathrm{s}^{-1}$ and shift slightly to a lower temperature (≈ 18 K). Viewing this change with regard to the general accuracy limitations of experimentally determined rate constants, it appears to be rather insignificant. In the context of the present study, however, which intends to present an accurate implementation of the most rigorous theory available by now, a change in the absolute rate constant value of approximately 50 percent should certainly be taken into account, even if it turns out to be unimportant for the HeH_2^+ association. It can actually be expected that for other more strongly bound systems the role of the cutting factor becomes more decisive. In this discussion of the importance of different sources from which the total rate constant is composed, it should also be mentioned that the contributions from broad resonances are not negligible. They are evaluated together with the contributions from free states, which increases the computational effort necessary in the rate constant calculations because a much larger number of evaluations of these free-bound transition amplitudes becomes unavoidable.

The big differences between the temperature curves for the rates of formation of the *para*- and *ortho* species of HeH_2^+ and their different contributing constituents as they are displayed in the lower two panels of Fig. 4 are mostly due to the shift of their dissociation limits. Looking in these panels at the comparison of the total rates with the contributions from sharp high J level ($J>7$) resonances, it can be noticed that for the HeH_2^+(*para*) these contributions amount to even more than 50 percent in the maximum region. Since the effect of resonances is generally rapidly decreasing with increasing temperature, the resonance contributions to the rate constant of the *ortho* species are much smaller. There is in this case instead a larger effect from the higher J levels of the first series ($[v]=1$) of states with ($p=1,k=0$).

VIII. CONCLUSIONS

The present study presents the first rigorous detailed state-to-state quantum calculation of a triatomic radiative association reaction for the relatively weakly interacting atom–diatom system $He+H_2^+$. It is assumed in the calculations that the reaction (2) is a so-called single-state process, i.e., that it is completely determined by the ground electronic

state potential of HeH_2^+ and that adiabatic couplings to excited states are negligible over the entire range of the potential surface relevant for the association process. It is further assumed that the higher dissociation channel leading to $HeH^+ + H$ can be neglected because it opens only at energies exceeding by far the collision energies considered here. Under these assumptions reliable predictions for the radiative association rate constant as a function of temperature are made for the low temperature interval $2 \leqslant T \leqslant 100$ K.

Due to the rather small binding energy of the ground electronic state of the HeH_2^+ ion, the rate constant for the $He + H_2^+$ radiative association was expected to be too small for any astrophysical implication. It is, however, an important result of this study that the small energy gain in the radiative stabilization of the association process is partly compensated by the larger number of resonance contributions enhancing the rate constant value. This supports previous statements in earlier theoretical studies[29–31] about the importance of resonances and it will have a strong impact on forthcoming theoretical studies of radiative association processes in other weakly interacting atom–diatom systems. In the $He^+ + H_2$ association, for instance, taking place on the potential energy surface of the electronically first excited state of the HeH_2^+ ion, calculations show that an even larger number of sharp resonances exist. It will therefore be interesting to study their influence on the two-state radiative association formation of the ground electronic state according to $He^+ + H_2 \rightarrow HeH_2^+(X\,^2A') + h\nu$, and even more interesting to see their role in the astrophysically relevant radiative charge transfer reaction (1). Another useful aspect of these studies of weakly interacting systems is that the detailed insight in the processes obtained here will be useful in similar studies of more strongly bound systems where, due to the rapidly increasing density of states, approximations have to be applied in order to make the calculations feasible. The present calculations on HeH_2^+ provide benchmark results which can be used to test these approximations.

In this context it appears that the detailed overview of the methodology applied in the present work to study the dynamics of the radiative association process (2) at low energies can serve as a useful reference in future calculations.

ACKNOWLEDGMENTS

This study was initiated when F.M. and V.Š were visiting the Max-Planck-Institute of Astrophysics in 2001. They are grateful for financial support and hospitality. This work was partly supported by the Grant Agency of the Academy of Sciences of the Czech Republic (Grant No. A4040806). W.P.K. is grateful for the invitation to visit the J. Heyrovský Institute of Physical Chemistry (Prague) in 2002, where the final version of the manuscript was completed.

[1] M. Kimura and N. F. Lane, Phys. Rev. A **44**, 259 (1991).
[2] A. Dalgarno, in *Physics of Electronic and Atomic Collisions*, edited by S. Datz (North-Holland, Amsterdam, 1982), p. 1.
[3] R. Johnsen, A. Chen, and M. A. Biondi, J. Chem. Phys. **72**, 3085 (1980).
[4] R. L. C. Wu and D. G. Hopper, Chem. Phys. **57**, 385 (1981).
[5] H. Boehringer and F. Arnold, J. Chem. Phys. **84**, 1459 (1986).
[6] M. M. Schauer, S. R. Jefferts, S. E. Barlow, and G. H. Dunn, J. Chem. Phys. **91**, 4593 (1989).
[7] M. Baer, S. Suzuki, K. Tanaka, H. Nakamura, Z. Herman, and D. J. Kouri, Phys. Rev. A **34**, 1748 (1986).
[8] B. Maiti, C. Kalyanaraman, A. N. Panda, and N. Sathyamurthy, J. Chem. Phys. **117**, 9719 (2002).
[9] P. Palmieri, C. Puzzarini, V. Aquilanti, G. Capecchi, S. Cavalli, D. de Fazio, A. Aguilar, X. Giménez, and J. M. Lucas, Mol. Phys. **98**, 1835 (2000).
[10] A. Carrington, Science (Washington, DC, U.S.) **274**, 1327 (1996).
[11] A. Carrington, D. I. Gammie, A. M. Shaw, S. M. Taylor, and J. M. Hutson, Chem. Phys. Lett. **260**, 395 (1996).
[12] D. I. Gammie, J. C. Page, and A. M. Shaw, J. Chem. Phys. **116**, 6072 (2002).
[13] M. F. Falcetta and P. E. Siska, Mol. Phys. **97**, 117 (1999).
[14] M. Meuwly and J. Hutson, J. Chem. Phys. **110**, 3418 (1999).
[15] W. P. Kraemer, V. Špirko, and O. Bludský, Chem. Phys. **276**, 225 (2002).
[16] R. J. Furlan, G. Bent, and A. Russek, J. Chem. Phys. **93**, 6676 (1990).
[17] W. P. Kraemer, M. Juřek, and V. Špirko, in *Advanced Series in Physical Chemistry*, edited by D. Papoušek (World Scientific, Singapore, 1997), p. 516.
[18] L. M. Bass, R. D. Cates, M. F. Jarrold, N. J. Kirchner, and M. T. Bowers, J. Am. Chem. Soc. **105**, 7024 (1983).
[19] E. Herbst, Astrophys. J. **313**, 867 (1987).
[20] E. Herbst, J. Chem. Phys. **70**, 2201 (1978).
[21] R. Loudon, *The Quantum Theory of Light* (Clarendon, Oxford, 1982).
[22] R. G. Newton, *Scattering Theory of Waves and Particles* (Springer, New York, 1966).
[23] Ch. J. Joachain, *Quantum Collision Theory* (North-Holland, Amsterdam, 1975).
[24] L. C. Biedenharn and J. D. Louck, *Angular Momentum in Quantum Physics* (Addison-Wesley, Reading, MA, 1981).
[25] G. G. Balint-Kurti and M. Shapiro, Chem. Phys. **61**, 137 (1981).
[26] G. G. Balint-Kurti and M. Shapiro, Adv. Chem. Phys. **60**, 403 (1985).
[27] R. D. Levine, *Quantum Mechanics of Molecular Rate Processes* (Clarendon, Oxford, 1969).
[28] D. L. Cooper, K. Kirby, and A. Dalgarno, Can. J. Phys. **62**, 1622 (1984).
[29] F. H. Mies, J. Chem. Phys. **51**, 787 (1969).
[30] R. E. Roberts, R. B. Bernstein, and C. F. Curtiss, J. Chem. Phys. **50**, 5163 (1969).
[31] R. A. Bain and J. N. Bardsley, J. Phys. B **5**, 277 (1972).
[32] L. Frommhold and H. M. Pickett, Chem. Phys. **28**, 441 (1978).
[33] D. R. Flower and E. Roueff, Astron. Astrophys. **72**, 361 (1979).
[34] M. Kimura, N. F. Lane, A. Dalgarno, and R. G. Dixon, Astrophys. J. **405**, 801 (1993).
[35] M. Juřek, V. Špirko, and W. P. Kraemer, Chem. Phys. **193**, 287 (1995).
[36] A. M. Lane and R. G. Thomas, Rev. Mod. Phys. **30**, 257 (1958).
[37] U. Fano, Phys. Rev. **124**, 1866 (1961).
[38] H. Feshbach, Ann. Phys. **5**, 357 (1958); **19**, 287 (1962).
[39] G. Brocks, A. van der Avoird, B. T. Sutcliffe, and J. Tennyson, Mol. Phys. **50**, 1025 (1983).
[40] F. T. Smith, J. Chem. Phys. **38**, 1304 (1963).
[41] F. T. Smith, Phys. Rev. **118**, 349 (1960).
[42] F. Mrugała and R. Moszynski, J. Chem. Phys. **109**, 10823 (1998).
[43] G. Brocks, J. Tennyson, and A. van der Avoird, J. Chem. Phys. **80**, 3223 (1984).
[44] M. Šindelka, V. Špirko, and W. P. Kraemer, Theor. Chem. Acc. (to be published).
[45] B. R. Johnson, J. Comput. Phys. **13**, 445 (1973).
[46] F. Mrugała, Int. Rev. Phys. Chem. **12**, 1 (1993).
[47] F. Mrugala, J. Chem. Phys. **115**, 3155 (2001).
[48] J. Tennyson and S. Miller, J. Chem. Phys. **87**, 6648 (1987).
[49] V. Špirko and W. Kraemer, J. Mol. Spectrosc. **172**, 265 (1995).
[50] M. Juřek, V. Špirko, and W. Kraemer, J. Mol. Spectrosc. **182**, 364 (1997).
[51] D. J. Kouri, in *Atom–Molecule Collision Theory*, edited by R. B. Bernstein (Plenum, New York, 1979), p. 301.
[52] M. Meuwly and J. Hutson, Mon. Not. R. Astron. Soc. **302**, 790 (1999).